A Major Role for hERG in Determining Frequency of Reentry in Neonatal Rat Ventricular Myocyte Monolayer

Luqia Hou, MS*[1,2], Makarand Deo, PhD*[1], Philip Furspan, PhD[1], Sandeep V. Pandit, PhD[1], Sergey Mironov, PhD[1], David S Auerbach, MS[1,4], Qiuming Gong, MD, PhD[3], Zhengfeng Zhou, MD, PhD[3], Omer Berenfeld PhD[1], José Jalife, MD[1,2]

Online Supplement

Methods

Adenoviral Construct

We generated adenoviral constructs containing WT or G628S cDNA sequence of hERG tagged with GFP, using the AdEasy vector system (Stratagene, La Jolla, CA) as described in[10] and in the online supplement (OLS) Viruses were purified using a kit (Virus Purification Kit, Clonetech) and the titer calculated (Rapid Titer Kit, Clontech) before multicellular preparations were infected with varying multiplicities of infection (MOI). MOIs of 200 and 30 were found to be optimal for uniform expression of WT and mutant hERG channels, respectively, based on the GFP level across the monolayer. An adenovirus carrying the sequence of GFP (Ad-GFP) at an MOI=10 served as control. All viral infections were performed after 48 hours in culture. After infection, the myocytes were cultured for an additional 48 hours to allow sufficient protein expression before mapping or patch-clamping.

Pacing Protocol

Monolayers were paced using 5-ms pulses at 2X threshold through a thin bipolar electrode. Incremental pacing started at 1 Hz, until loss of 1:1 capture or induction of sustained reentry. The I_{Kr} blocker, E4031 (1 μM) was superfused when indicated.

Data Analysis

Single Cell Electrophysiology: We used commercially available software (pCLAMP, version 10.2; Axon Instrument, Forster City,CA). I_{Kr} peak pulse currents were measured using the Clampfit subroutine of the pCLAMP software, normalized to cell capacitance, and plotted against voltage.

Optical Movies: Ensemble averaging at each pixel was performed over 5 or more propagating wavefronts synchronized with stimuli. Background fluorescence was subtracted from each frame, and spatial (3x3 pixels) and temporal (7 pixels) conical convolution filters were applied. Dominant frequency (DF) maps and phase maps were constructed in monolayers showing sustained reentry as described.[3,4,11] Optical APDs were measured at 80% repolarization. The local CV was measured as described.[12] Briefly, the distributions of activation times (50% of upstroke) for the spatial regions of 5x5 pixels were fitted with the plane, and gradients of activation times gx and gy were calculated for each plane along the *x* and *y* axes, respectively.

The magnitude of the local CV was calculated for each pixel as $(g_x^2 + g_y^2)^{-1/2}$. Mean values and standard deviations for CV and APD were calculated for the entire visible surfaces and for sequential activations. During pacing, wavelength (WL) was calculated as WL = APD x CV. However, it is well known that during functional reentry both APD and CV vary greatly as a function of distance from the center of rotation (core).[3] Therefore, during sustained reentry, the WL was measured from the phase maps as the expanse between the wavefront and the end of the repolarization wavetail, at a fixed distance of 10 mm from the core (see Online Supplement for details).

Supplemental Experimental Data:

The methods for the construction of phase maps, activation maps and time-space plots have been described in great detail previously.[1-5]

Online Figure I presents color activation maps of sustained reentry corresponding to the phase maps shown in Figure 2 of the main article. Neonatal rat ventricular monolayers were infected with Ad-GFP, Ad-hERG, or Ad-G628S. In Online Figure II, we illustrate the original optical signals and corresponding time-space plots for the same experiments. Each time-space plot (bottom) was constructed along the horizontal white line drawn on the equivalent reentry snapshot (top). Please note that Ad-hERG significantly abbreviated the spatial extension of the excited state (white) and greatly accelerated reentry frequency, as reflected by the large increase in the number of rotations in the respective time-space plot. In contrast Ad-G628S appreciably increased the spatial extension of the excited state and reduced the number of rotations in the time-space plot.

Online Figure III shows examples of single pixel recordings at pacing cycle lengths between 1000 and 200 ms. The excellent signal-to-noise ratio shown by all examples provides evidence of our ability to accurately measure APD at three different levels (30, 50 and 80%) of repolarization.

We determined the role of wavefront curvature in determining the changes of reentry frequency and dynamics secondary to hERG modification, as illustrated in panel A of Online Figure IV: 1) A snapshot of the phase movie showing a rotor with a singularity point (SP) at its pivoting tip was randomly selected for each of a total of n=9 monolayers in each group. 2) In each snapshot we determined by visual inspection the orientation of the wavefront tip in the immediate vicinity (i.e., within 3 pixels) of the SP. 3) We then drew a line in that orientation across the SP. 4) Subsequently, we drew a second line perpendicular (90 degree angle) to the SP crossing line and extended it to approximate the first ½ winding of the wavefront; i.e., to the nearest transition between phases blue and purple in the phase map. 5) We measured the length of the second line. 6) We took that length being equivalent to the diameter of a hemi-circle approximately delineating the wavefront in its first ½ winding and therefore as being inversely proportional to its curvature at that location.

Mathematical Modeling

We have modified an existing mathematical model of neonatal rat myocyte by Korhonen et al.[6] This model is unique in that cytosolic Ca^{2+} is a function of temporal as well as spatial coordinates. Due to lack of t-tubules,[7] calcium ions entering the cells via membrane channels have to diffuse a small distance through the cytosol before reaching the sarcoplasmic reticulum (SR) and trigger the excitation-contraction coupling (ECC) machinery. The following ionic current components were modified in order to reproduce the AP morphology and restitution properties recorded from the experiments performed in our laboratory. Other formulations in the Korhonen model[6] remain unchanged.

Fast Na^+ current (I_{Na})

The formulation for the fast Na^+ current was based on a mammalian ventricular myocyte model (LRd 1999).[8] The maximum conductance of the current (G_{Na}) was adjusted to obtain a maximum dV/dt (135 mV/ms) and AP amplitude (91 mV) in the range of our experimentally recorded values. The voltage dependence of I_{Na} steady-state inactivation and activation were modified to fit our experimental data in neonatal rat ventricular myocytes (see Online Figure V; n=16, measured at 22 ^{o}C). The inactivation curves (*h* and *j* gates) were shifted by +2 mV to compensate for the temperature-dependent changes in the I_{Na} kinetics (Q_{10} compensation).[9] An additional +10 mV shift was introduced in the steady-state inactivation to compensate for the liquid junction potentials and extrapolation to the physiological $[Na]_o$ concentration (154 mM).[9] Thus, the fast Na^+ current was modeled as:

$$I_{Na} = G_{Na} m^3 h j (V - E_{Na})$$

$$\tau_x = \frac{1}{(\alpha_x + \beta_x)}$$

where x in the subscript can be *m*, *h* or *j*. E_{Na} is the reversal potential for sodium.

$$\alpha_m = 0.32 \frac{V + 47}{1 - e^{-0.1(V+47)}}$$

$$\beta_m = 0.08 e^{\frac{V}{-11}}$$

If $V < -40$ mV,

$$\alpha_h = 0.135 e^{\frac{80+V}{-6.8}}$$

$$\beta_h = 3.56 e^{0.079V} + 310000 e^{0.35V}$$

$$\alpha_j = 2.0 \times \left(-127140 e^{0.2444V} - 0.00003474 e^{-0.04391V}\right) \frac{(V + 37.78)}{\left(1 + e^{0.311(V+79.23)}\right)}$$

$$\beta_j = \frac{0.1212 e^{-0.01052V}}{1 + e^{-0.1378(V+40.14)}}$$

And if $V \geq -40$ mV,

$$\alpha_h = \alpha_f = 0$$

$$\beta_h = \frac{1}{0.13\left(1 + e^{\frac{V+10.66}{-11.1}}\right)}$$

$$\beta_f = \frac{0.3e^{-0.0000002535V}}{\left(1 + e^{-0.1(V+32)}\right)}$$

Time-independent K^+ current

The formulation for the time-independent K^+ current (I_{K1}) was modified in accordance to our experimental data (n=5). Online Figure VI shows the I-V plots for I_{K1} from experiments and the modified NRVM model. Note that the experimental values have been shifted by -10mV to compensate for the liquid junction potential errors. The resulting I_{K1} formulation is as follows:

$$I_{K1} = k_{IK1} \times 0.0515 \times \frac{[K^+]_o}{[K^+]_o + 210} \times \frac{V - E_K - 6.1378}{0.1653 + e^{0.0321(V - E_K - 6.1378)}}$$

The value of k_{IK1} was set to 2.0 to match the recorded peak inward I_{K1} density in our experiments.

Cytosolic Calcium transients

The cytosolic calcium transients in Korhonen model[6] vary between 200 nM (diastolic) and 700 nM (systolic). We reduced the absolute amplitudes to lie between 250 nM and 500 nM during diastole and systole, respectively (see below). This was achieved by reducing the maximum Ca^{2+} release from ryanodine receptors (RyR) (k_{RyR}) by 50%.

L-type calcium current (I_{CaL})

I_{CaL} formulation involves a voltage-dependent activation gate (d), a voltage-dependent inactivation gate (f) and one $[Ca^{2+}]_i$-dependent inactivation gate (f_{Ca}).[6] In order to compensate for the reduced $[Ca^{2+}]_i$ distributions, the steady-state curve of Ca^{2+}-dependent inactivation ($f_{Ca_{ss}}$) was reduced to match the original formulation by ten-Tusscher et al.[10] Thus the f_{Ca} gate was formulated as follows:

$$f_{Ca_{ss}} = \frac{\alpha_{fCa} + \beta_{fCa} + \gamma_{fCa} + 0.23}{1.46}$$

where,

$$\alpha_{fCa} = \frac{1}{1 + \left(\frac{[Ca^{2+}]_{subSL}}{0.000325}\right)^8}$$

$$\beta_1 fCa = 0.1 \times 1/(1 + e^1(([\,[Ca]\,^{\uparrow}(2+)\,]_1 subSL - 0.0005)/0.0001))$$

$$\gamma_1 fCa = 0.2 \times 1/(1 + e^1(([\,[Ca]\,^{\uparrow}(2+)\,]_1 subSL - 0.00075)/0.0008))$$

$[Ca^{2+}]_{subSL}$ is the subsarcolemmal calcium concentration.

Delayed rectifier K^+ Currents, I_{Kr} and I_{Ks}

Rapid component of the delayed rectifier K^+ current, I_{Kr}, exhibits rapid activation and prominent inward rectification. We replaced the I_{Kr} formulation in the Korhonen model by a formulation based on Luo-Rudy dynamic (LRd 1995) model of ventricular myocyte.[11] It consists of a time-dependent activation gate, X_r, and a time-independent inactivation gate, R, to approximate very rapid inactivation process of this channel. I_{Kr} is thus expressed as:

$$I_{Kr} = g_{Kr} \cdot X_r \cdot R \cdot (V - E_K)$$

where, E_K is the reversal potential of potassium and g_{Kr} is the maximum conductance of I_{Kr} which exhibits a square root dependence on extracellular potassium concentration ($[K^+]_o$) and is expressed as

$$g_{Kr} = 0.0005228\sqrt{\frac{[K^+]_o}{5.4}}$$

Online Figure VII shows normalized I_{Kr} densities recorded experimentally and reproduced by the computer model for control and for I_{Kr} upregulation The g_{Kr} was scaled by a factor of 5.21 (obtained from our experimental recordings) to reproduce the I_{Kr} densities in hERG overexpressed myocytes.

The gating variables X_r and R are governed by,

$$X_{r\infty} = \frac{1}{1 + e^{-\frac{V+21.5}{7.5}}}$$

$$\tau_{Kr} = \frac{1}{\left(\frac{0.00138(V+14.2)}{1 - e^{-0.123(V+14.2)}} + \frac{0.00061(V+38.9)}{e^{(0.145(V+38.9)-1)}}\right)}$$

$$R = \frac{1}{1 + e^{\frac{V+9}{22.4}}}$$

The slow component, I_{Ks}, was adapted from LRd 1999 model[8] which consists of two activation processes, represented by a fast gate, X_{s1} and a slow gate, X_{s2}.

$$I_{Ks} = g_{Ks} \cdot X_{s1} \cdot X_{s2} \cdot (V - E_{Ks})$$

Where g_{Ks} is the maximum conductance of I_{Ks}, which is cytosolic calcium-dependent. We replaced the intracellular calcium concentration in the original formulation with the subsarcolemmal concentration, $[Ca^{2+}]_{subSL}$. Thus the g_{Ks} is expressed as

$$g_{Ks} = 0.0866 \times \left(1.0 + \frac{0.6}{1 + \left(\frac{0.000038}{[Ca^{2+}]_{subSL}}\right)^{1.4}}\right)$$

The gating variables X_{s1} and X_{s2} are governed by,

$$X_{s1_\infty} = X_{s2_\infty} = \frac{1}{1 + e^{\frac{V - 1.5}{16.7}}}$$

$$\tau_{Xs1} = \frac{1}{\left(\frac{7.19 \times 10^{-5} \times (V + 30)}{1 - e^{-0.148(V+30)}} + \frac{1.31 \times 10^{-4} \times (V + 30)}{e^{0.0687(V+30)} - 1}\right)}$$

$$\tau_{Xs2} = 4 \times \tau_{Xs1}$$

E_{Ks} in the I_{Ks} expression is the reversal potential computed by the following expression

$$E_{Ks} = \left(\frac{RT}{F}\right) \times \ln\left(\frac{[K^+]_o + P_{Na,K} \times [Na^+]_o}{[K^+]_i + P_{Na,K} \times [Na^+]_i}\right)$$

where $P_{Na,K} = 0.01833$ is the Na/K permeability ratio.

Online Table I lists the modified parameters used in our NRVM model. Initial conditions for the modified parameters are given in Online Table II.

Computer Simulations:

The modified NRVM computer model was used to study the effects of I_{Kr} overexpression in single cell and 2D monolayer simulations. The single-cell model was first paced for 50 sec to attain steady state and the values of all state variables were saved. These steady state values were used as initial conditions for all the simulations. For single cell simulations, the model was paced at varying frequencies (from 1 to 20 Hz). After attaining steady state for 20 sec, the APs

and fast inward sodium current (I_{Na}) were recorded in the last 3 sec. hERG overexpression was implemented by scaling I_{Kr} by a factor of 5.21 (5.21X), which was derived from our experiments (see Online Figure VII). Peak I_{Na} was plotted against pacing frequency for each case. In yet another set we scaled I_{Ks} (25X) with normal I_{Kr}. Differences in cell excitability in terms of peak I_{Na} amplitude were investigated in both sets. The cell excitability was also studied by pacing the single cell model (Control and I_{Kr} 5.21X) at 2 Hz for 10 seconds (S1) followed by a premature stimulus (S2). The timing of S2 was varied between 10 ms and 100 ms after the repolarization due to the last S1 and the peak I_{Na} was recorded. A similar protocol was used to study the effects of cell excitability on the conduction velocity along a 10 mm long cable for both the cases. We also used a disk-shaped 2D geometry, 35 mm in diameter, to simulate a NRVM monolayer. The disc was constructed with a resolution of 100 μm per computational cell (total = 95,093 cells). Reentry was induced via cross-field stimulation and the DF was determined as in the experiments. We used a similar protocol to induce reentry in the I_{Kr} 5.21X monolayer. A subset of simulations was performed by clamping the minimum diastolic potential at less negative values during reentry I_{Kr} 5.21X monolayer models to study the effects of transient hyperpolarization on the conduction velocity and the frequency of reentry.

Simulated action potentials:

Action potential (AP) parameters recorded from experiments using patch-clamp techniques and those obtained from the modified NRVM computer model are listed in Online Table III. The simulated single-cell APs were elicited by injecting a stimulus current of -100 pA/pF (duration 0.5 ms) at 1 Hz pacing frequency. The amplitude of the simulated APs was approximately 91 mV, which is in line with our experiments. Our model reproduced the neonatal rat ventricular myocyte AP morphology in agreement with the experiments and with previous studies.[6,12]

Online Figure VIII shows the experimental and simulated AP traces and the intracellular calcium transients in the model for 1Hz pacing. The Ca^{2+} ions enter the cell via sarcolemmal (SL) channels (L- and T-type Ca^{2+} channels) and diffuse through the cytosol to reach the SR which is an important feature of the Korhonen model.[6] Therefore, the cytosolic Ca^{2+} concentrations at SL and SR differ slightly as seen in the figure. Online Figure IX shows the APD restitution curves for the model and experimental data, measured at 80% repolarization (APD_{80}). The protocol for restitution included pacing the modified NRVM model for 20 sec for each pacing frequency before measuring APD_{80}.

In summary, our modified model is able to closely mimic our experimental single cells action potentials. This model was then used to explore the consequences of overexpression of I_{Kr} in the monolayers, as reported in the main article.

Role of the transient hyperpolarization

Our experimental data suggest that in addition to the APD abbreviation, hERG overexpression results in a transient hyperpolarization after each action potential which contributes to the observed increased rotation frequency. To provide further support to that hypothesis, we conducted additional simulations. In panel A of Online Figure X, we present results using S1-S2 protocol in a 1D cable (10 mm) to measure changes in conduction velocity (CV). Similar to what

we demonstrated experimentally (see Fig. 7C), upregulating I_{Kr} 5.21X increased CV at all S1-S2 intervals. However, CV did not increase when the resting membrane potential was clamped to -70 mV. As shown in panel B, IKr upregulation increased the frequency of reentry in the monolayer model. As expected, the frequency of reentry was progressively reduced when the level of the clamped voltage was progressively depolarized. Altogether, the results strongly support the role of the transient hyperpolarization in addition to the APD abbreviation in increasing the rotor frequency and CV during reentry in I_{Kr} upregulation.

Method of measuring the wavelength (WL)

As shown in Online Figure XI, WL during reentry was defined by the length of the black line drawn on the phase map 10 mm from the center of rotation (white circle) and perpendicular to the tangent at the wavefront (blue).[4] In both experiments (panel A) and simulations (panel B) I_{Kr} upregulation reduced WL significantly during sustained reentry.

Figures and Tables

Online Table I. Modified parameters and their values in our NRVM model

Parameter	*Definition*	*Value*
g_{Na}	Maximum I_{Na} conductance	6.3 mS/µF
g_{CaL}	Maximum I_{CaL} conductance	5.67×10^{-5} dm^3/(F ms)
k_{RyR}	Scaling factor for J_{RyR}	0.005 ms^{-1}
k_{IK1}	Scaling factor for I_{K1}	2.0
k_{NCX}	Scaling factor for I_{NCX}	1.1340×10^{-16} pA/(pF (µm)^4)
I_{NaK}^{max}	Maximum NaK-ATPase current	3.1995 pA/pF
g_{Nab}	INab conductance	0.0039 mS/µF

Online Table II. Initial conditions for the modified formulations

Parameter	*Definition*	*Value*
V	Membrane potential	-72.79684 mV
m	I_{Na} activation gating variable	0.015898145552
h	I_{Na} fast inactivation gating variable	0.947273505079
j	I_{Na} slow inactivation gating variable	0.908486044987
X_r	I_{Kr} time-dependent activation gating variable	0.025742210977
X_{s1}	I_{Ks} fast activation gating variable	0.012668791315
X_{s2}	I_{Ks} slow activation gating variable	0.028399873909
$[Na^+]_i$	Intracellular Na^+ concentration	13818.5982638 µM
$[K^+]_i$	Intracellular K^+ concentration	150953.3914836 µM
$[Ca^{2+}]_{subSL}$	Subsarcolemmal Ca^{2+} concentration	0.2626943 µM
$[Ca^{2+}]_{subSR}$	Cytosolic Ca^{2+} concentration near SR	0.2630095 µM

Online Table III. Comparison of the AP characteristics of the NRVM model with the experimental values

Parameter	Experiments	Model
MDP (mV)	-72.09±2.5	-72.7968
AP amplitude (mV)	98.82±11.75	91.65
APD30 (ms)	80±26.99	95.0
APD50 (ms)	113.98±44.59	112.5
APD80 (ms)	166.88±34.43	129.7

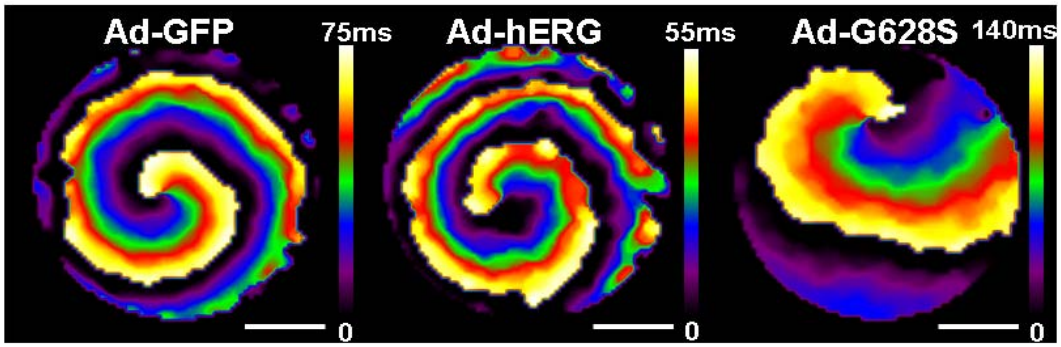

Online Figure I. Activation maps of the NRVM monolayers infected with Ad-GFP, Ad-hERG, or Ad-G628S. Scale bar on the right of each map indicates different time point as shown in different color. Scale bars in white: 10mm.

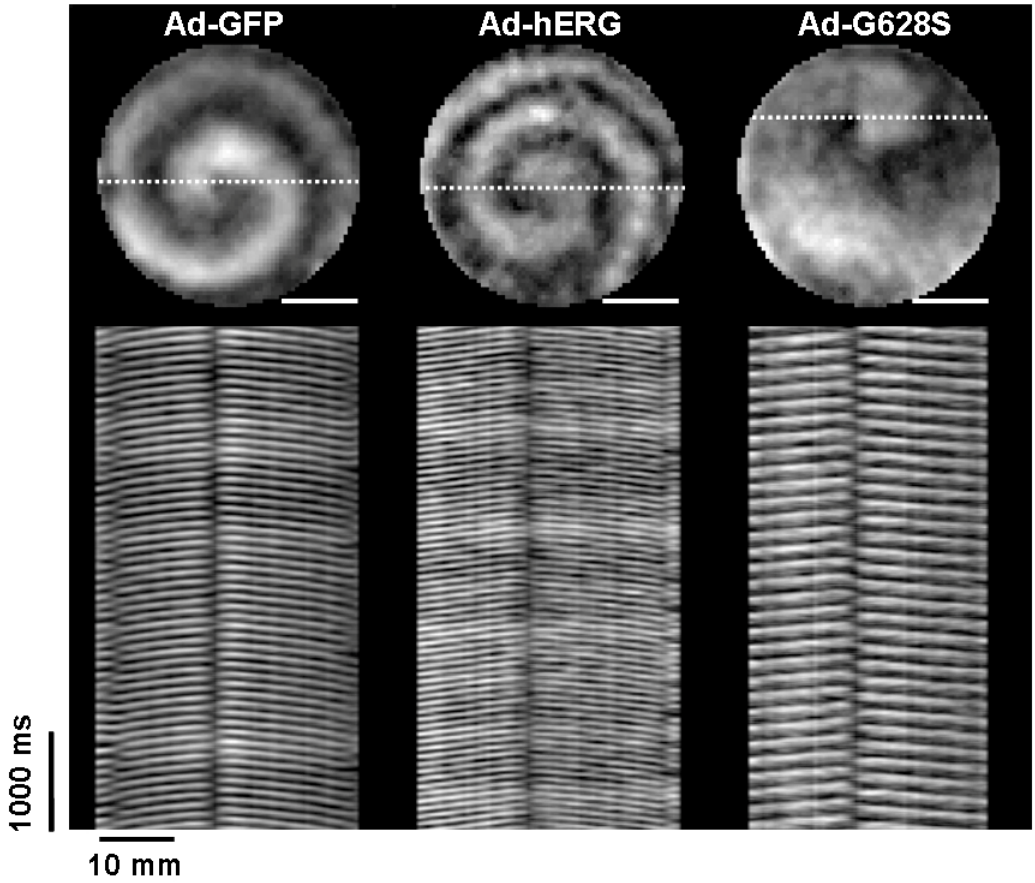

Online Figure II. Optical signals and time-space plot (TSP) show the singularity points in monolayers infected with Ad-GFP, Ad-hERG, or Ad-G628S. TSPs were constructed for activity recorded along the horizontal white lines in the optical recordings. Scale bars in white: 10mm.

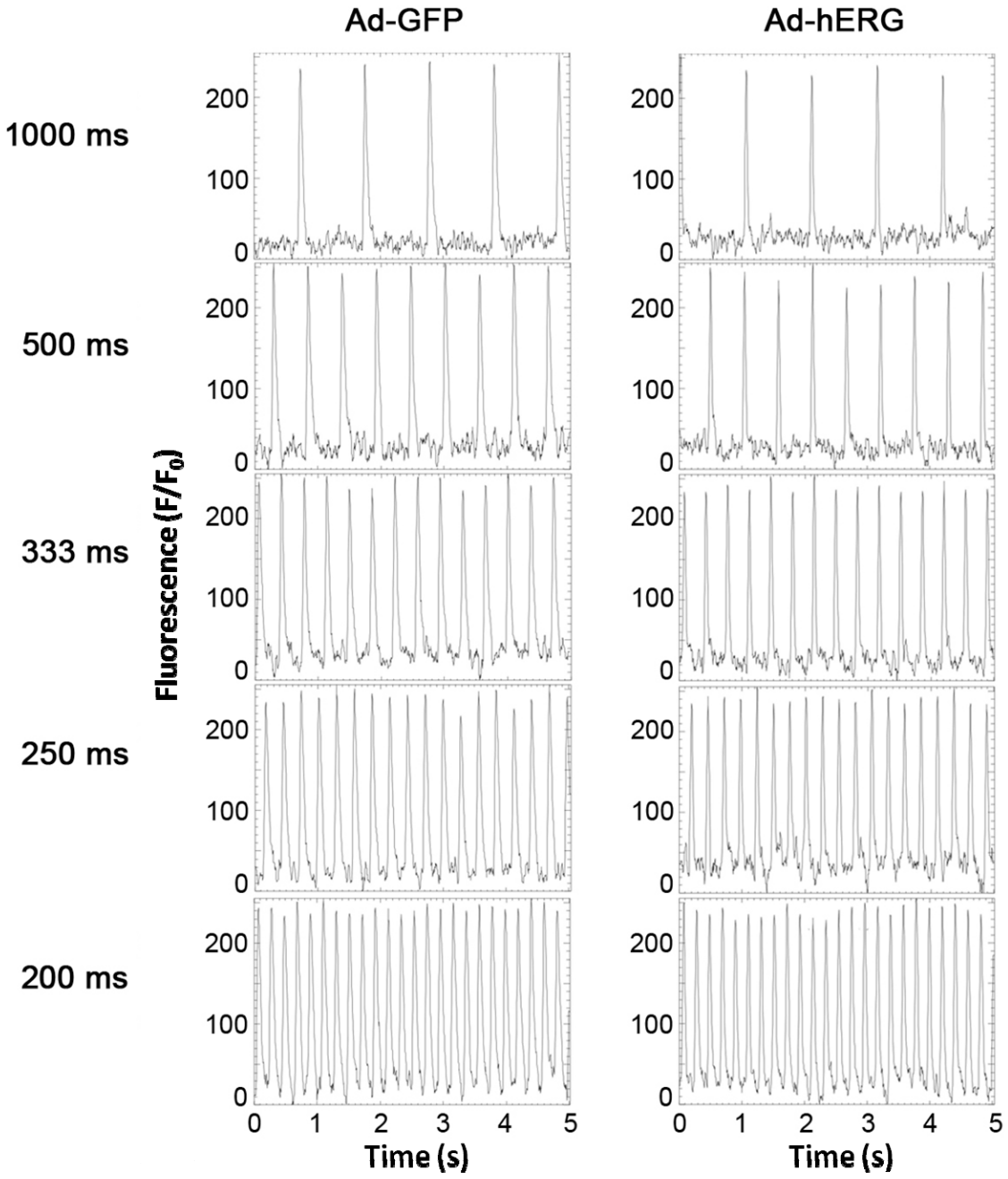

Online Figure III. Single pixel recordings from Ad-GFP and Ad-hERG infected monolayers under pacing cycle length of 1000ms, 500ms, 333ms, 250ms, and 200ms.

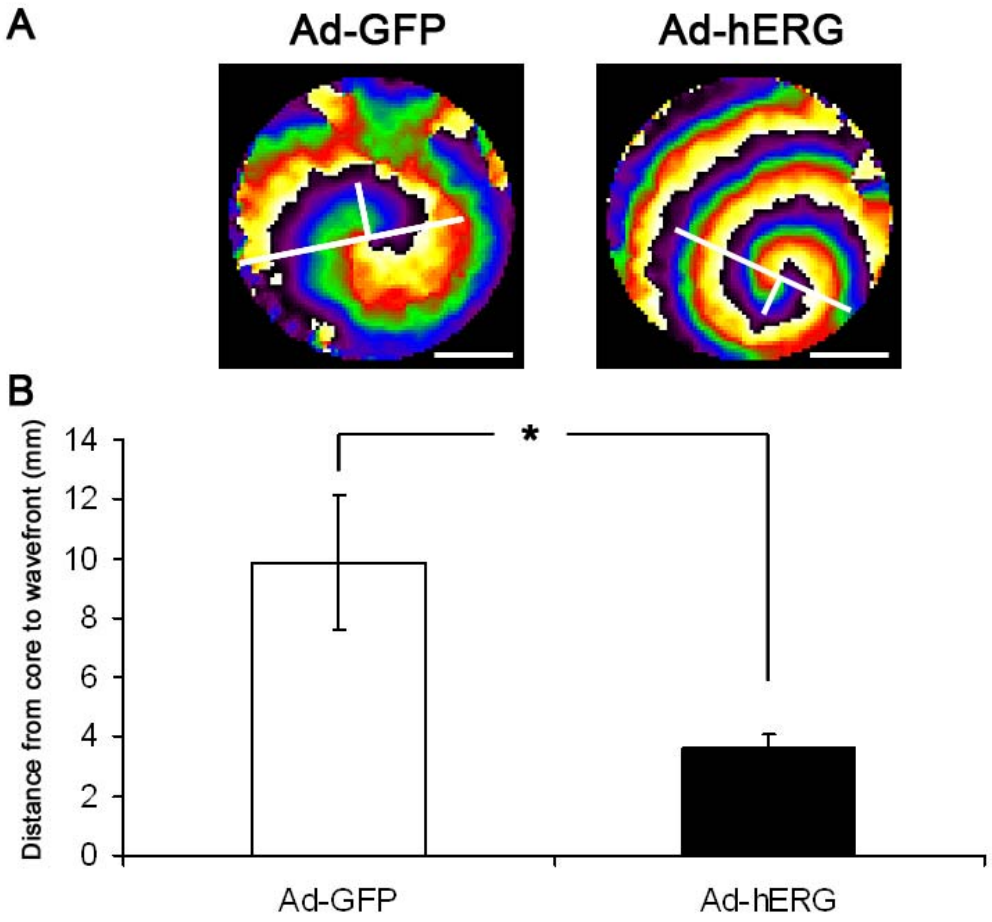

Online Figure IV. Rotor curvature in monolayers infected with Ad-GFP and Ad-hERG. Panel A, Snapshots of the phase movies in Ad-GFP and Ad-hERG infected monolayers. White lines indicated the distance between the tip of rotating spiral wave (Singularity point at center of core) to the wavefront at ½ of the spiral wave full winding (the boundary between blue and purple bands – see text). Scale bar: 10 mm; Panel B, quantification of the distance between the core and the wavefront. *: $p<0.05$. Long white lines: The orientation of the wavefront at the tip. Short white lines: Orientaion perpendicular to the wavefront at the tip; used to measure the tip-to-½ winding distance.

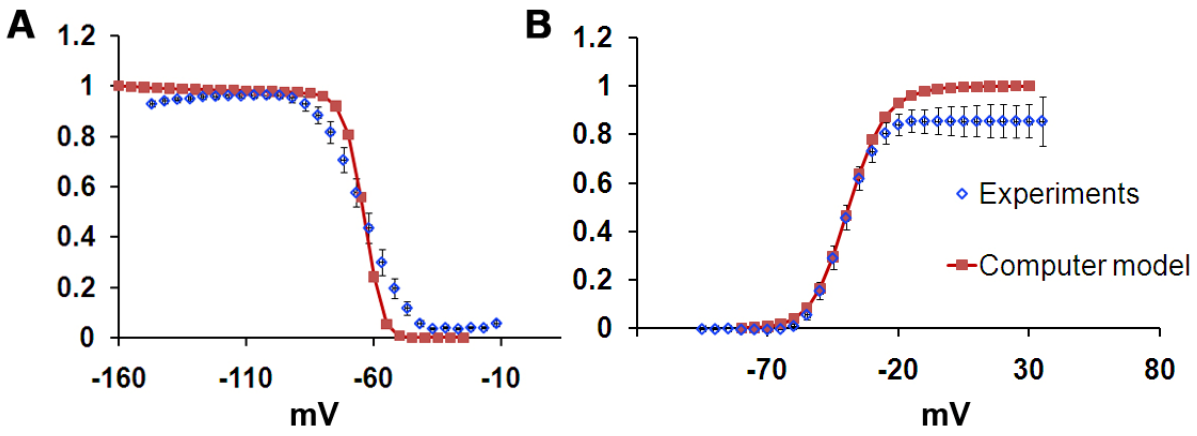

Online Figure V. (A) Voltage dependence of I_{Na} inactivation and (B) activation kinetics of the model were adjusted to our experimental recordings (n=16). The error bars represent ±SEM.

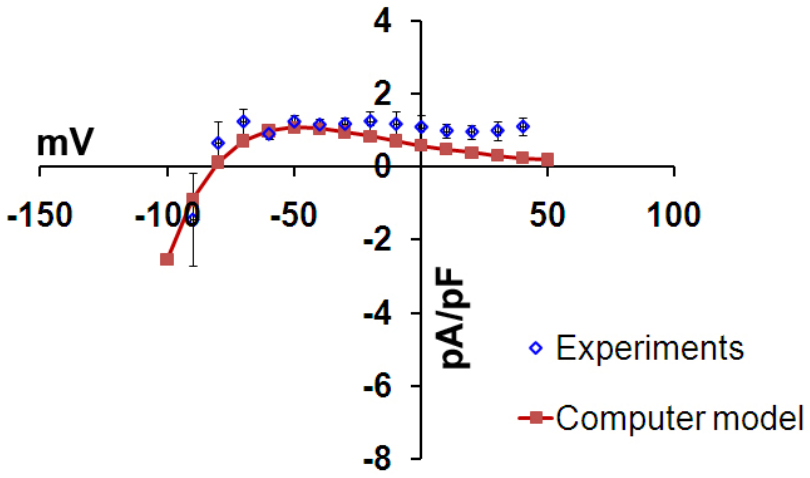

Online Figure VI. The inward rectifier potassium current (I_{K1}) in our NRVM model was modified according to the experimentally recorded I-V relationship (n=6). The error bars represent ±SEM.

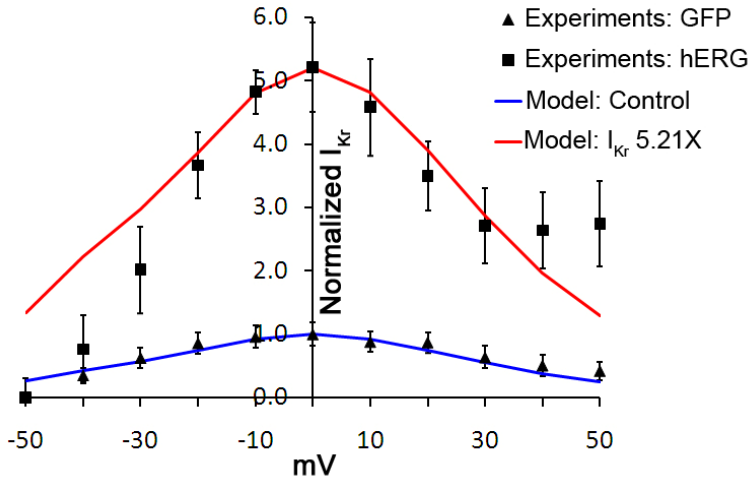

Online Figure VII. Normalized I_{Kr} current density in the modified NRVM model was adjusted according to experimental recordings in control and hERG overexpressed (I_{Kr} 5.21X) myocytes.

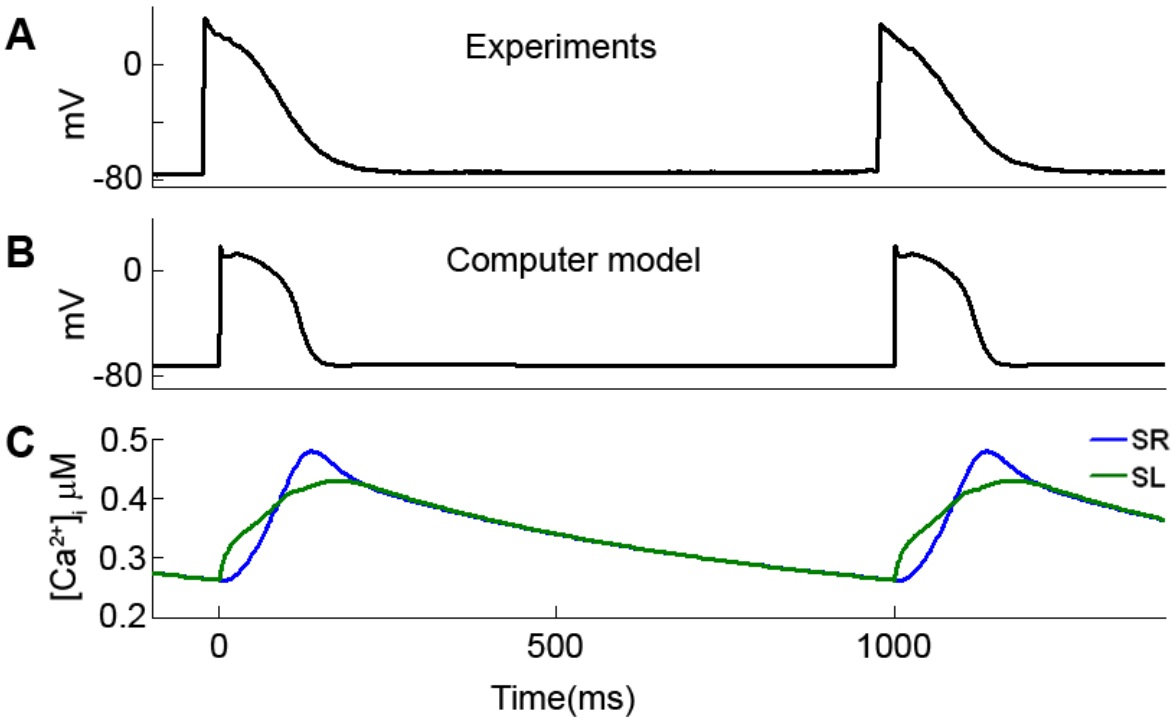

Online Figure VIII. (A) Action potentials recorded in our experiments during 1 Hz pacing. (B) Action potentials elicited by 1 Hz pacing stimulus in our NRVM computer model. (C) Temporal distribution of cytosolic calcium at subsarcolemmal (SL) and near sarcoplasmic reticulum (SR) during pacing.

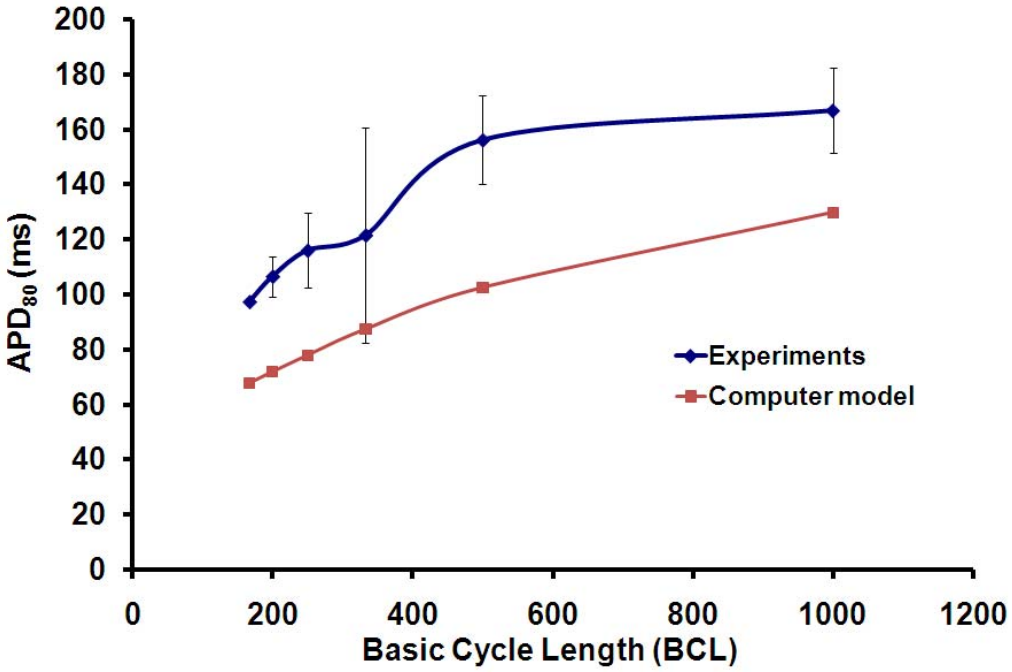

Online Figure IX. The computer model reproduced experimentally observed APD restitution properties. The error bars represent standard error.

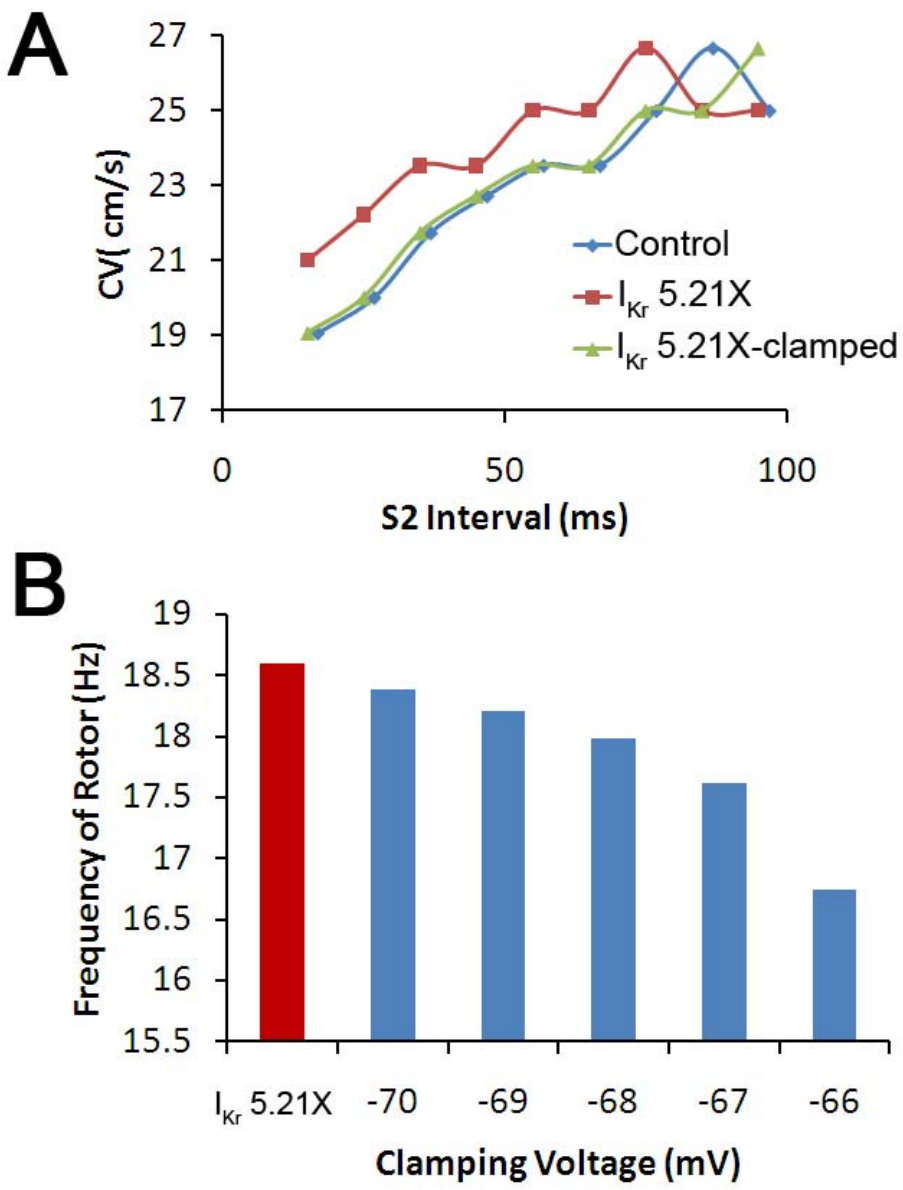

Online Figure X. Effects of transient hyperpolarization in the I_{Kr} 5.21X model. **A.** The same S1-S2 protocol as in Fig. 7C was used in a 1D cable of 10 mm length. The increase in I_{Na} was translated into proportional increase in CV for all S2 intervals. Note that the increase in CV was not observed when the MDP was clamped to -70 mV. **B.** The frequency of reentry in 2D I_{Kr} 5.21X monolayer model decreased progressively when the MDP was clamped to more positive voltages, thus indicating the role of transient hyperpolarization in accelerating reentry.

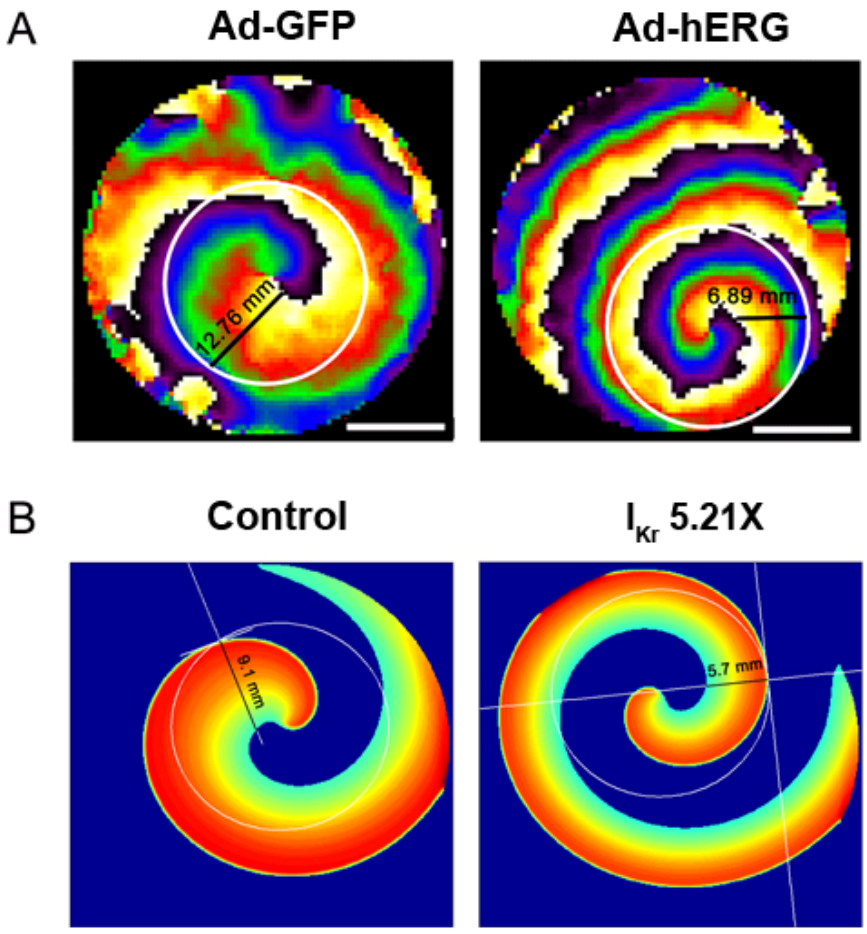

Online Figure XI. Wavelength measurement in experiments (A) and simulations (B). A, Snapshots of the phase movies in Ad-GFP and Ad-hERG infected monolayers. White circles indicated the distance of 10 mm from the center of the reentry. In each panel, WL is given by the length of the black line extending between the wavefront (blue) and the end of repolarization wavetail (yellow). Scale bar: 10 mm; B, Snapshots of the voltage map in control and I_{Kr} 5.21X monolayers in simulation.

References:

1. Gray RA, Pertsov AM, Jalife J., Spatial and temporal organization in cardiac fibrillation. *Nature*. 1998; 392:75-78.

2. Samie FH, Berenfeld O, Anumonwo J, Mironov SF, Udassi S, Beaumont J, Taffet S, Pertsov AM, Jalife J**.** Rectification of the Background Potassium Current. A Determinant of Rotor Dynamics in Ventricular Fibrillation. *Circ Res*. 2001; 89:1216-1223.

3. Noujaim SF, Pandit SV, Berenfeld O, Vikstrom K, Cerrone M, Mironov S, Zugermayr M, Lopatin AN, Jalife J. Up-regulation of the inward rectifier K+ current (IK1) in the mouse heart accelerates and stabilizes rotors. *J Physiol.* 2007; 578:315-326.

4. Munoz V, Grzeda KR, Desplantez T, Pandit SV, Mironov S, Taffet SM, Rohr S, Kleber AG, Jalife J. Adenoviral expression of IKs contributes to wavebreak and fibrillatory conduction in neonatal rat ventricular cardiomyocyte monolayers. *Circ Res.* 2007; 101:475-483.

5. Zlochiver S, Muñoz V, Vikstrom KL, Taffet SM, Berenfeld O, Jalife J. Electrotonic myofibroblast-to-myocyte coupling increases propensity to reentrant arrhythmias in two-dimensional cardiac monolayers. *Biophys J*. 2008; 95:4469-80.

6. Korhonen T, Hanninen SL, Tavi P, Model of Excitation-Contraction Coupling of Rat Neonatal Ventricular Myocytes. *Biophysical J*. 2009; 96:1189–1209.

7. Delcarpio JB, Claycomb WC, Moses RL. Ultrastructural morphometric analysis of cultured neonatal and adult-rat ventricular cardiac-muscle cells. *Am J Anat.* 1989; 186:335–345.

8. Viswanathan PC, Shaw RM, Rudy Y. Effects of IKr and IKs heterogeneity on action potential duration and its rate dependence: a simulation study. *Circulation*. 1999; 99:2466-74.

9. Colatsky TJ. Voltage clamp measurements of sodium channel properties in rabbit cardiac Purkinje fibres. *J Physiol*. 1980; 305:215-34.

10. ten Tusscher, KHWJ, Noble D, Noble PJ, Panfilov AV. A model for human ventricular tissue. *Am. J. Physiol. Heart Circ. Physiol*. 2004; 286:H1573–H1589.

11. Zeng J, Laurita KR, Rosenbaum DS, Rudy Y. Two Components of the Delayed Rectifier K+ Current in Ventricular Myocytes of the Guinea Pig Type. *Circ Res*. 1995; 77:140-152.

12. Gaughan JP, Hefner CA, Houser SR. Electrophysiological properties of neonatal rat ventricular myocytes with alpha1-adrenergic-induced hypertrophy. *Am J Physiol*. 1998; 275:H577-90.